

# Context-Aware Target Classification with Hybrid Gaussian Process prediction for Cooperative Vehicle Safety systems

Rodolfo Valiente\*, Arash Raftari\*, Hossein Nourkhiz Mahjoub\*

Mahdi Razzaghpour\*, Syed K. Mahmud\*\*, Yaser P. Fallah\*

\*Connected and Autonomous Vehicle Research Lab (CAVREL)

Department of Electrical and Computer Engineering, University of Central Florida, Orlando, FL, USA

\*\*Hyundai America Technical Center, Inc. (HATCI)

Superior Township, MI, USA

*Abstract*—Vehicle-to-Everything (V2X) communication has been proposed as a potential solution to improve the robustness and safety of autonomous vehicles by improving coordination and removing the barrier of non-line-of-sight sensing. Cooperative Vehicle Safety (CVS) applications are tightly dependent on the reliability of the underneath data system, which can suffer from loss of information due to the inherent issues of their different components, such as sensors' failures or the poor performance of V2X technologies under dense communication channel load. Particularly, information loss affects the target classification module and, subsequently, the safety application performance. To enable reliable and robust CVS systems that mitigate the effect of information loss, we proposed a Context-Aware Target Classification (CA-TC) module coupled with a hybrid learning-based predictive modeling technique for CVS systems. The CA-TC consists of two modules: A Context-Aware Map (CAM), and a Hybrid Gaussian Process (HGP) prediction system. Consequently, the vehicle safety applications use the information from the CA-TC, making them more robust and reliable. The CAM leverages vehicles' path history, road geometry, tracking, and prediction; and the HGP is utilized to provide accurate vehicles' trajectory predictions to compensate for data loss (due to communication congestion) or sensor measurements' inaccuracies. Based on offline real-world data, we learn a finite bank of driver models that represent the joint dynamics of the vehicle and the drivers' behavior. We combine offline training and online model updates with on-the-fly forecasting to account for new possible driver behaviors. Finally, our framework is validated using simulation and realistic driving scenarios to confirm its potential in enhancing the robustness and reliability of CVS systems.

*Index Terms*—Context-Aware Target Classification, Cooperative Vehicle Safety Systems, Gaussian Process, Scalable V2X communication.

## I. INTRODUCTION

In a Cooperative Vehicle Safety (CVS) system, Connected and Autonomous Vehicles (CAV) take advantage of the data acquired from communication to extend their situational awareness and improve safety [1]–[3]. In CVS systems, Remote Vehicles (RV) frequently broadcast their state infor-

mation to the neighboring vehicles over a wireless channel in the form of an information message, e.g., Basic Safety Messages (BSM) [4], [5] using Vehicle-to-Everything (V2X) communication. V2X communication allows the information from RVs to be available at the Host Vehicle (HV) over the wireless network extending the situational awareness of CAVs and alleviating the limitations of the sensor-based systems that rely on line-of-sight sensing [6]–[8]. At the HV, the information messages are processed to monitor the neighboring road participants and create a real-time map of all objects in its vicinity. The crash warning algorithms and other safety applications access the real-time map regularly to identify potentially dangerous situations. Therefore, the V2X communication technologies have a significant impact on the accuracy of safety applications. In that sense, two major V2X technologies, Cellular-V2X (C-V2X) and Dedicated Short-Range Communication (DSRC) have been developed [9], [10]. Nevertheless, they suffer from information loss and have scalability limitations in real-time applications affecting the quality of the real-time map and the CVS system's performance [4], [5], [11], [12].

CVS architectures separate the design of applications from the communication system allowing flexibility and simpler adoption of different communication technologies. Figure 1 shows a CVS system that consists of a communication and sensor layer, a Target Classification (TC) layer, and a safety application layer [13], [14]. TC classifies the neighboring RVs based on their relative locations with respect to the HV. While the safety applications have been extensively studied [8], [13]–[16], there are limited studies on TC [17], [18]. Current TC solutions are limited in their context-awareness and prediction capabilities, making them vulnerable to communication losses, subsequently affecting the performance of the safety applications [17], [18].

To address this challenge we present a Context-Aware Target Classification (CA-TC) module for mitigating the effect of communication loss or sensor failure. The CA-TC fits within the CVS system block and consists of two modules: a Context-Aware Map (CAM) and a Hybrid Gaussian Process

This material is based upon work partially supported by the National Science Foundation under Grant No. CNS-1932037, NSF CAREER Grant 1664968 and in part by the Hyundai America Technical Center, Inc. (HATCI).

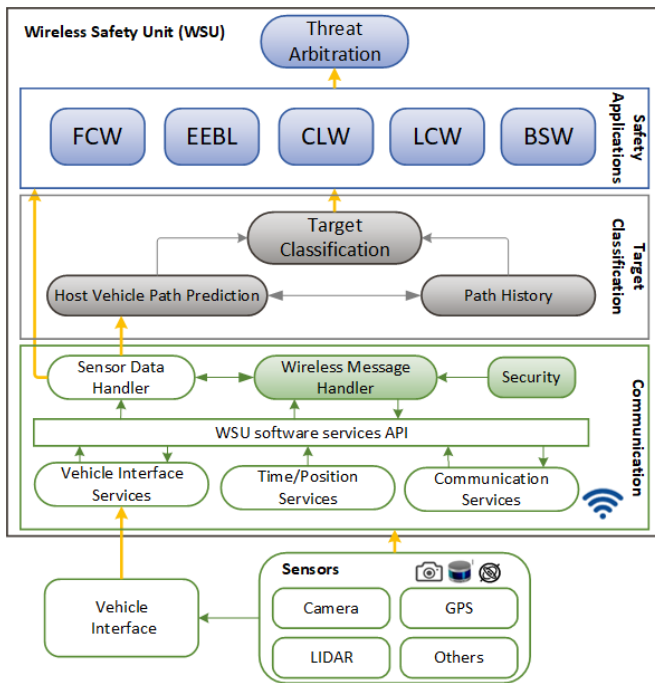


Fig. 1: Cooperative Vehicle Safety system block diagram.

(HGP) prediction system as shown in Figure 2. The CAM module separates application and information/perception subsystems and leverages vehicles' path history, road geometry, tracking, and prediction. The prediction module is a non-parametric Bayesian inference modeling scheme, Gaussian Process regression, and is responsible for vehicle's trajectory predictions when data is not received due to communication losses or sensor failure. The prediction system allows the CA-TC to precisely predict future behaviors and compensate for information loss. In this paper, we focus on improving the TC layer in Figure 1. While we particularly proposed a suitable prediction method for our architecture, the CA-TC allows the use of any prediction method to address the aforementioned challenge.

Our main contributions are as follows:

- We proposed a Context-Aware Target Classification module for CVS systems that alleviate the effect of information loss on the performance of safety applications.
- A novel Hybrid-learning-based Gaussian Process prediction method is presented. It relies on a bank of driver models learned from real data in an offline manner to perform forecasting on-the-fly, while also allowing online updates of the driver models, accounting for new possible driving behavior.
- The proposed system is evaluated in a simulation and hardware-in-the-loop utilizing a Remote Vehicle Emulator (RVE) based on a DSRC Wireless Safety Unit (WSU), which facilitates the analysis of the CVS applications and the communication system performance. Additionally, we study the impact of using different prediction techniques and demonstrate the performance gains caused by the

proposed prediction method.

## II. LITERATURE REVIEW

### A. Cooperative Vehicle Safety Systems

CVS systems are an active area of research in vehicle safety [18]–[21]. In [22], [23] the information from V2X communication is used for increased situational awareness and improve safety, and authors in [17], [24] present a CVS system that continuously tracks all RVs in the vicinity of the HV. CVS systems rely on the accuracy of the real-time map of RVs which is processed by the safety applications to identify potential threats. The architecture must be modular and flexible enough to allow variations in communication rate and sensor limitations [25].

Figure 1 presents a CVS system architecture [13], [14]. The modules include the services modules, WSU software API, sensors and wireless data handler, the TC, and safety applications. The WSU software services modules are generic modules supplied by the WSU that provide services and an API to enable applications to interface to the CAN bus, GPS receiver, and wireless. Based on the data from surrounding vehicles, the TC classifies the locations of the RVs within a specified radius of the HV and provides relative position and velocity metrics for the classified RVs. The application modules consist of multiple Vehicle-to-Vehicle (V2Vs) applications and evaluate potential safety threats based on inputs from the system framework modules [13].

### B. Cooperative Vehicle Safety Applications

Different from non-cooperative safety applications that depend on the line-of-sight sensors, cooperative perception systems leverage the information accessible through V2V communication to identify the presence and location of the RVs increasing the perception range. In the vehicle safety communication report from NHTSA [13], [14] the main cooperative safety applications within CVS were described, such as Cooperative Forward Collision Warning (FCW), Control Loss Warning (CLW), Emergency Electronic Brake Lights (EEBL), Blind Spot Warning (BSW), Lane Change Warning (LCW) among others. In [26] a Cooperative Vehicle-to-Pedestrian safety application is implemented to provide extended situational awareness and threat detection, reducing crashes and improving safety. Authors in [27] present a cooperative testing platform to evaluate the efficacy of CVS applications under challenging conditions and a Collision Warning Avoidance (CWA) system is presented and evaluated in [28].

### C. Target Classification (TC)

In order to realize the above-mentioned safety applications, the surrounding vehicles should be tracked and classified. While the safety applications have been widely explored, the TC layer has received less attention [17], [18]. However, it is a main component in the CVS architecture and the performance of all the applications relies on an accurate and robust TC [17], [18]. In that direction, a machine learning-based TC for Millimeter-Wave Radar is proposed in [29], it uses an artificial

neural network and convolutional neural network (CNN) and shows acceptable performance in a specific domain. In [18] a TC layer is proposed to classify the RVs with respect to the HV, which considers road geometry, the local map, the path history, and a simple vehicle tracking algorithm based on a Kalman filter. These approaches are limited in their prediction capabilities making them vulnerable to communication losses and sensor failures. In order to mitigate these issues, we propose a CA-TC layer and a robust and suitable prediction approach for the TC layer.

#### D. Tracking and Prediction

In order to overcome CVS performance degradation caused by non-ideal communication, methods for tracking and predicting information have been proposed [30]–[34]. The constant speed or acceleration model is the most frequently accepted assumption for prediction by conventional vehicle manufacturers. The fundamental rationale for using those models is the standardization of the BSM communication rate to 10Hz, given the short time between BSM the models remain valid under ideal communication channels. Nevertheless, because of the limitations of communication technology, the assumption is not always valid in real scenarios, particularly in heavily congested situations [35].

Kalman filters have been also used widely for tracking position and velocity [31], [32]. This is likely due to the relative simplicity and robust nature of the filter itself. In [33] is presented an adaptive KF to predict vehicle velocity, the approach is tested in a variety of driving scenarios showing a good performance in velocity prediction.

More recent effective approaches for trajectory prediction include recurrent neural networks [36], [37], gaussian mixture models [38], [39] and Long Short-Term Memory NNs [40], [41]. In [40] is described an LSTM model to predict vehicle trajectories, leveraging the LSTM network to infer the temporal relationship from previous sequence data. Authors in [40] propose a coupling LSTM model to effectively predict the future trajectories of vehicles. The LSTM network can learn the temporal relation from the historical sequence data and is employed as the basic prediction model for all vehicle trajectories with common parameters. Following the recent developments in that field of generative models, several works make use of autoencoder-based solutions [42], [43], proposing solutions that include Recurrent Variational Autoencoder, Conditional Variational Autoencoder or Generative Adversarial Network [42], [43]. Autoencoders have been used effectively to learn a better representation and for a prediction task in previous works [44]–[46]. In [44] a predictive autoencoder is proposed to produce future observation, predicting velocity map images directly and kinematics predictions using a the predictive autoencoder. Authors in [47] present a variational autoencoder used for prediction with partial interpretability. The proposed model achieves good performance, however, the expensive training cannot be done on-the-fly while new data is available, which makes it harder to learn from current information and adapt to new scenarios.

To address those challenges we propose a novel hybrid learning approach based on Bayesian inference. By leveraging non-parametric Bayesian approaches we can predict fundamental patterns of observable time series and capture coupled driver/vehicle dynamics without enforcing any assumptions on the model parameters. This extraordinary feature frees the learning process from the constraints of certain function patterns. The complexity of a model created in a non-parametric Bayesian inference framework is automatically adjusted to the observed data, allowing it to avoid over-complex models while still capturing unforeseen patterns in the data on-the-fly. Particularly, within the non-parametric Bayesian inference approaches, Gaussian Process (GP) has demonstrated a significant performance improvement in terms of packet generation rate as well as position tracking accuracy under network congestion [34]. GP attempts to regress observed time-series realizations by projecting a prior distribution directly over the function space, rather than the function parameters space, in such a way that any finite subset of draws from this distribution represents a multivariate Gaussian random vector [48]. This approach adjusts the model complexity to the observed data, allowing it to capture distinct patterns as they arise during training. This idea has been utilized in [49], [50] to enhance the performance of Cooperative Adaptive Cruise Control (CACC) in congested traffic scenarios.

Previous works have demonstrated that within the context of Model-Based Communication (MBC), a modeling scheme that uses GP as its inference technique outperforms other modeling approaches [34], [51]. Different from other works that provide a transmitter-side approach using GP for prediction via an MBC paradigm we propose a receiver-side approach that leverages GP to forecast the trajectories of the RV, therefore, the proposed architecture does not require modifications in the current V2X standards.

### III. CONTEXT-AWARE TARGET CLASSIFICATION (CA-TC)

In this section, we present the CA-TC. The CA-TC fits within the CVS system block in Figure 1. The proposed CA-TC is presented in Figure 2 and consists of the HV path prediction, the path history of all vehicles, the current received BSMs from RVs (Local Map), a tracking module, and the HGP system, all of which are integrated into the CAM, in which data fusion, history, and predictions are used for lane estimation and local map reconstruction creating a real-time context map of the surroundings. By leveraging tracking and prediction, CA-TC provides accurate information that improves the performance of safety applications. The CA-TC enables the applications to work based on the CAM rather than individual BSMs or sensory data. Using the CAM, the RVs are classified based on the relative current and predicted location with respect to HV. Therefore, it allows the safety applications to be triggered not just by the local map and history but also based on the predictions, either when packages are lost or when the prediction system detects a possible warning. For instance, as an illustration in Figure 2, the local map is showing RV1 as behind, but the CAM is predicting RV1

will be behind right, so RV1 will be also processed by LCW and BSW safety application to check possible future hazards based on the CA-TC information. The proposed CA-TC allows applications to be independent of underlying communication and sensing systems, and the architecture is adaptable to new sensing technologies.

In the CA-TC (Figure 2), the map-update module (Local Map) is in charge of refreshing the real-time map with the latest received information from sensors, GPS, and communication module. Thus, the real-time map database keeps the records of its surrounding entities, such as all neighboring vehicles, and other detected objects. Every local map record consists of the latest available information about a particular neighboring entity, such as its position information, speed, size, etc. The local map is created and updated based on the latest HV and RVs position. The path history (PH) module keeps track of HV and RVs history. It keeps a buffer of the vehicle's most recent position and sensor data points and computes concise representations of the vehicle's actual PH based on the allowable position error tolerance between the actual vehicle path and its concise representation, and updates the PH concise representation periodically for use by the other modules. The HV path prediction module makes use of the HGP prediction algorithm to forecast the future path of the HV. The tracking module utilizes the HGP prediction algorithm together with the previous and current local map information to correct the vehicle's position, recover current missed RVs and filter possible outliers. The HGP prediction system uses the information from PH, tracking, and current local map records for future path prediction points for all vehicles. By having an accurate RV prediction, the CA-TC allows safety applications to be triggered based on forecasting and not just current received information.

All the aforementioned modules are used by the CAM for an extended situational awareness subsystem that is responsible for delivering the latest and most accurate information to the safety application to identify present and future possible threats and generate appropriate notifications and signals. While the CAM can leverage information from local sensors and V2X communication, in this work, we focus on the communication side and study the impact of communication imperfections on CVS applications.

#### A. Target Classification

With the information provided by the CAM, the RVs are classified in different areas based on the relative locations with respect to the HV. In addition to the classification of RVs, the CA-TC also provides the vehicles' predictions, relative speeds, headings, lateral and longitudinal offsets, and tracking positions. Figure 4 shows the classification of the RVs relative to the HV. The CA-TC computes the RVs classifications area based on the longitudinal and lateral distances with respect to HV [17], [18]. based on the relatives' longitudinal distance the

RVs are classified as,

$$RV_{class} = \begin{cases} X_{rel} \geq 0, & \text{Ahead} \\ X_{rel} < 0, & \text{Behind} \end{cases} \quad (1)$$

Next the longitudinal distance classifications are combined with the relatives' lateral distance ( $ld$ ) information to classify the RVs as,

$$RV_{class} = \begin{cases} ld \in (1.5w_{lane}, \infty), & \text{Far Left} \\ ld \in (0.5w_{lane}, 1.5w_{lane}], & \text{Left} \\ ld \in [-0.5w_{lane}, 0.5w_{lane}], & \text{On Centre} \\ ld \in [-1.5w_{lane}, -0.5w_{lane}), & \text{Right} \\ ld \in (-\infty, -1.5w_{lane}), & \text{Far Right} \end{cases} \quad (2)$$

in which  $w_{lane}$  is the width of the lane. Finally, for the oncoming/ongoing traffic, the lane heading angle  $\phi_{lane}$  is compared with the RVs heading angle  $\phi_{RV}$  to classify the RVs as,

$$RV_{class} = \begin{cases} |\phi_{RV} - \phi_{lane}| \leq \Delta\phi_{ongoing}, & \text{Ongoing} \\ |\phi_{RV} - \phi_{lane}| \geq \Delta\phi_{oncoming}, & \text{Oncoming} \\ \text{else,} & \text{not classified} \end{cases} \quad (3)$$

where ongoing vehicles are vehicles in the same direction, and oncoming vehicles are vehicles in the opposite direction.  $\Delta\phi_{ongoing}$  and  $\Delta\phi_{oncoming}$  are the threshold values for classification. Based on these RV classifications the safety applications are evaluated. Figure 3 depicts the mapping of RV classification to various safety applications. Based on the data given by the CA-TC, the safety application modules independently analyze possible safety hazards. This demonstrates that appropriate TC is crucial for the triggering and functioning of safety applications, as the warnings are dependent on the RVs being classified correctly. For example, in the event of an approaching rear-end collision with a vehicle ahead in the same lane and direction of travel, the TC will classify the vehicle as Ahead and the FCW application will be evaluated as indicated in Figure 3.

#### IV. HYBRID-LEARNING-BASED GAUSSIAN PROCESS (HGP) PREDICTION SYSTEM

The prediction system is used at the HV (receiver side) to regress the observed time-series realizations from PH, capturing the distinct patterns as they emerge in the data. Each observation point is chosen from Gaussian random variables that are not independent and have temporal relationships with their predecessors and successors. The correlation describes the temporal relationship between observations, making GP a useful tool for detecting patterns in time series.

The set of  $m$  observed values is represented by an  $m$ -dimensional multivariate Gaussian random vector, which is defined by an  $m \times m$  covariance matrix and a  $m$  mean vector. This covariance matrix, often known as the GP kernel, is the foundation upon which GP detects and anticipates the underlying behavior of time series based on their recorded

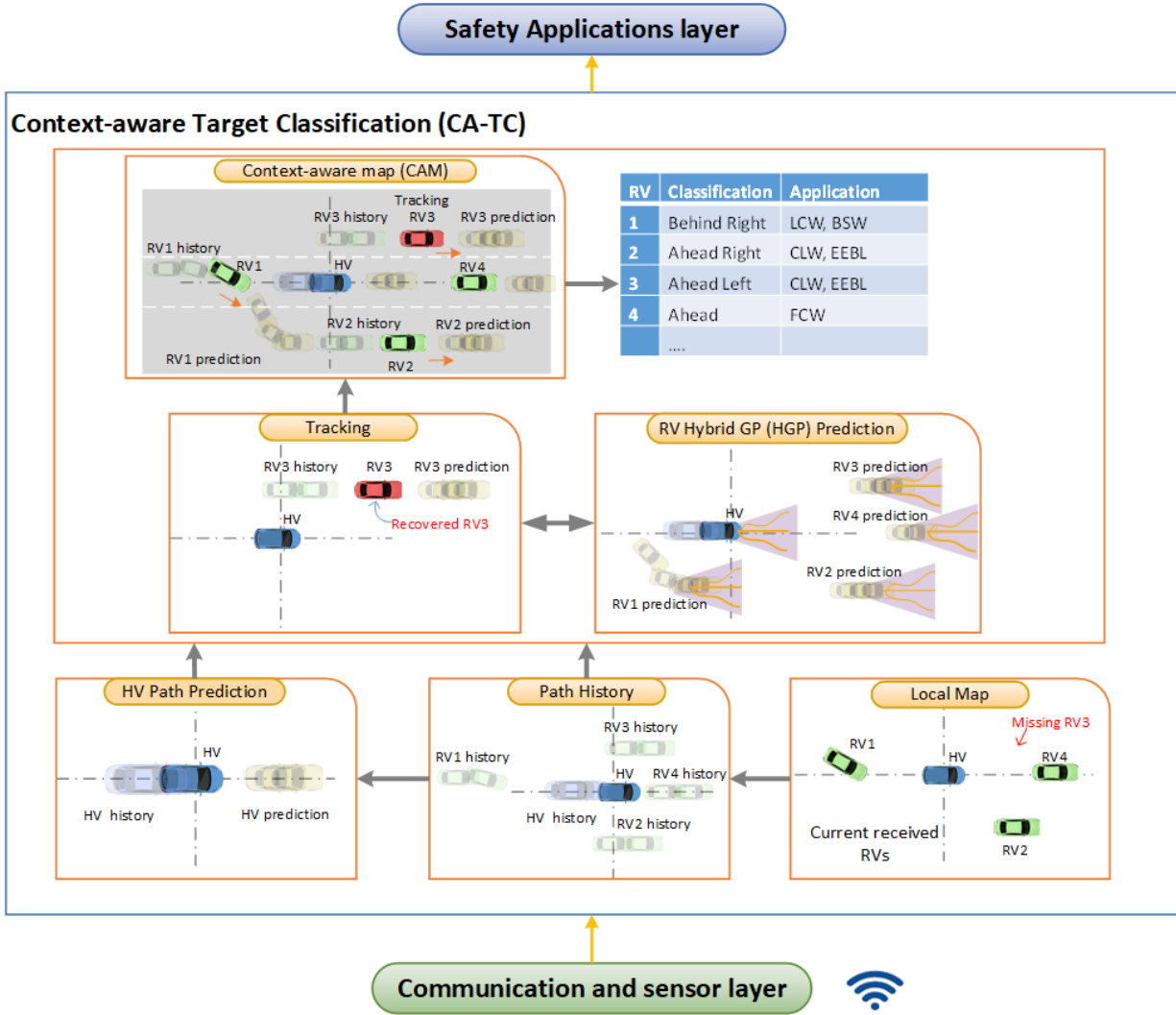


Fig. 2: Context-Aware Target Classification module with HGP prediction for CVS systems. The HGP prediction system is responsible for accurate vehicle predictions and the CAM leverages vehicles' path history, road geometry, tracking, and prediction to improve the robustness and reliability of the safety applications. In the figure, HV is in blue, RVs are in green, a missing RV is in red, predictions are in shadow yellow, and the vehicle's history is in shadow green.

history. The fundamental GP components can be expressed mathematically as follows,

$$\begin{aligned}
 f(t) &\sim gp(m(t), k(t, t')), \\
 \{X_i\}_{i=1,2,\dots,m} &= \{f(t_i)\}_{i=1,2,\dots,m} \sim \mathcal{N}(\mu, \Sigma), \\
 \mu &= [m(t_1), \dots, m(t_m)]^T, \\
 \Sigma_{ij} &= \kappa(t_i, t_j) \quad \forall i, j \in \{1, 2, \dots, m\},
 \end{aligned} \quad (4)$$

where  $X_i$ ,  $f(t)$ ,  $m(\cdot)$ , and  $\kappa(\cdot, \cdot)$  are the samples of the vehicles' state, observed or to be predicted at the time  $t_i$ , the unknown underlying function that the vehicles' states are sampled from, the mean and the covariance functions, respectively.

Instead of working directly with the position time series, the proposed inference algorithm treats the vehicles' heading and longitudinal speed as two independent time series that

are regressed using GPs. The proposed method is divided into two stages: Training and Forecasting. During the offline training procedure, the hyper-parameters of kernel functions are learned based on the observed samples of the vehicles' speed and heading to create a bank of vehicle/driver short-term behavioral models. The well-known realistic data set, Safety Pilot Model Deployment (SPMD) [52], is used for training and selecting a group of significant models that represent the data. It was shown through experiments that a limited-size kernel bank suffices to model joint vehicles' dynamic and driver behavior. Given the availability of this bank of models, during forecasting, the most recent information of RVs and path history is used to select the model with the highest likelihood from the bank and use it to forecast the vehicles' state until new information is received.

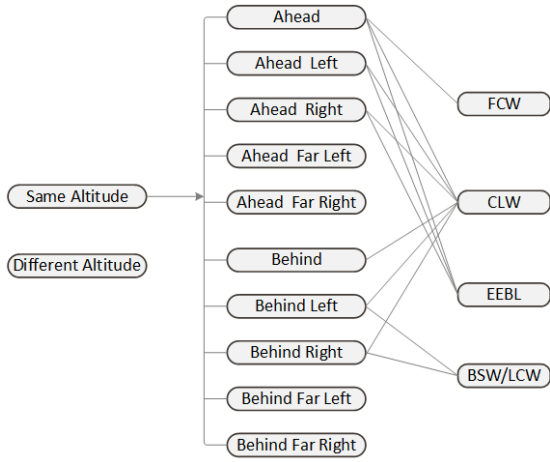


Fig. 3: Target Classifications areas used by the safety applications.

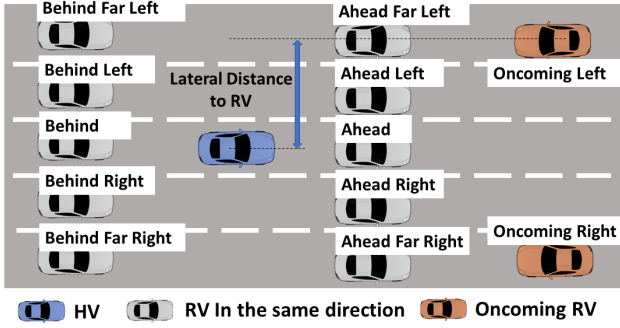


Fig. 4: Target Classifications of the RVs relative to the HV.

### A. Training

During training, the sequences of equally-spaced samples of longitudinal speed and heading, measured every  $100ms$ , with size  $TW = 30$  were used to learn the GP models and subsequently construct the kernel banks. In this work, based on the findings in [34], a compound kernel of Radial Basis Function (RBF) and a linear kernel is used as the covariance function and the mean function is considered to be zero. Therefore, the covariance function in (4) can be expressed as:

$$\kappa(t, t') = \alpha_1^2 \exp\left(-\frac{\|t - t'\|^2}{2\gamma^2}\right) + \alpha_2^2 tt'. \quad (5)$$

we used the Leave-One-Out cross-validation to learn a GP model and obtain the set of parameters  $\theta = \{\gamma, \alpha_1, \alpha_2\}$  for each under consideration sequence of speed or heading. Assuming the  $i^{th}$  element of the observed speed or heading sequence,  $x_i$ , is left out, the joint distribution of  $x_i$  and the rest of the sequence,  $\mathcal{X}_{-i}$ , can be expressed as:

$$\begin{bmatrix} x_i \\ \mathcal{X}_{-i} \end{bmatrix} \sim \mathcal{N}\left(\mathbf{0}, \begin{bmatrix} \kappa(t_i, t_i) & K_1^T(t_i, \mathbf{t}_{-i}) \\ K_1(t_i, \mathbf{t}_{-i}) & K_2(\mathbf{t}_{-i}, \mathbf{t}_{-i}) \end{bmatrix}\right), \quad (6)$$

where  $K_1$  is a  $(m-1) \times 1$  vector representing the covariance between  $\mathcal{X}_{-i}$  and  $x_i$ ,  $K_2$  is the  $(m-1) \times (m-1)$  covariance

matrix of  $\mathcal{X}_{-i}$ , and  $\mathbf{t}_{-i}$  represents the time stamps of  $\mathcal{X}_{-i}$ .  $K_1$  and  $K_2$  can be obtained using (5). The conditional probability of  $x_i$  given the rest of the sequence can be derived as

$$\begin{aligned} (\mathbf{x}_i | \mathbf{t}, \mathcal{X}_{-i}, \theta) &\sim \mathcal{N}(\mu_i, \sigma_i), \\ \mu_i &= \mathbf{K}_1^T[(t_i, \mathbf{t}_{-i}) | \theta] \mathbf{K}_2^{-1}[(\mathbf{t}_{-i}, \mathbf{t}_{-i}) | \theta] \mathcal{X}_{-i}, \\ \sigma_i &= -\mathbf{K}_1^T[(t_i, \mathbf{t}_{-i}) | \theta] \mathbf{K}_2^{-1}[(\mathbf{t}_{-i}, \mathbf{t}_{-i}) | \theta] \mathbf{K}_1[(t_i, \mathbf{t}_{-i}) | \theta] \\ &\quad + \kappa[(t_i, t_i) | \theta]. \quad (7) \end{aligned}$$

Therefore, the log probability of observing  $x_i$  given the rest of the sequence,  $(\mathcal{X}_{-i})$ , can be calculated as

$$\log p(x_i | \mathbf{t}, \mathcal{X}_{-i}, \theta) = -\frac{1}{2} \log \sigma_i^2 - \frac{(x_i - \mu_i)^2}{2\sigma_i^2} - \frac{1}{2} \log 2\pi \quad (8)$$

Defining the cross-validation objective function as the sum of the  $\log$  probabilities over all elements of the sequence, i.e.,  $L(\mathbf{t}, \mathcal{X}, \theta) = \sum_{i=1}^m \log p(x_i | \mathbf{t}, \mathcal{X}_{-i}, \theta)$ , the optimal parameters  $\theta = \{\gamma, \alpha_1, \alpha_2\}$ , for an under consideration sequence of vehicles' states, can be obtained using the conjugate gradient optimization method as proposed in [53].

In our settings, GPS information is converted into Earth-Centered, Earth-Fixed format (ECEF). The ECEF format is offset to the center of the vehicle on the ground and then transformed into East-North-Up (ENU) coordinates. As the heading and longitudinal speed of the vehicle are treated as two independent time series, we apply the GP regression technique to model and forecast the vehicles' speed and heading, and use the forecasted speed and heading to predict the position, we particularly call this approach indirect prediction. Given that the parameters of speed and heading kernel functions are obtained by optimizing the Leave-One-Out objective function using  $m$ -most recent observations of speed and heading data, the predictive distribution of future speed and heading values,  $\mathcal{S}^*$  and  $\mathcal{H}^*$ , conditioned on having observed speed and heading values,  $\mathcal{S}^{obs}$  and  $\mathcal{H}^{obs}$ , at time stamps  $\mathbf{t}$  can be derived as

$$\begin{aligned} (\mathcal{S}^* | \mathbf{t}^*, \mathbf{t}, \mathcal{S}^{obs}) &\sim \mathcal{N}(\mu_s^*, \Sigma_s^*), \\ \mu_s^* &= K_1[(t^*, t) | \theta_s] K_2^{-1}[(t, t) | \theta_s] \mathcal{S}^{obs}, \\ \Sigma_s^* &= -K_1[(t^*, t) | \theta_s] K_2^{-1}[(t, t) | \theta_s] K_1^T[(t, t^*) | \theta_s] \\ &\quad + K_3[(t^*, t^*) | \theta_s], \\ (\mathcal{H}^* | \mathbf{t}^*, \mathbf{t}, \mathcal{H}^{obs}) &\sim \mathcal{N}(\mu_h^*, \Sigma_h^*), \\ \mu_h^* &= K_1[(t^*, t) | \theta_h] K_2^{-1}[(t, t) | \theta_h] \mathcal{H}^{obs}, \\ \Sigma_h^* &= -K_1[(t^*, t) | \theta_h] K_2^{-1}[(t, t) | \theta_h] K_1^T[(t, t^*) | \theta_h] \\ &\quad + K_3[(t^*, t^*) | \theta_h], \quad (9) \end{aligned}$$

where  $K_3$ ,  $K_2$  and  $K_1$  are the covariance matrices between future (predicted) values, observed values and observations, and future values respectively, and can be derived using (5). Using the predictive distributions of longitudinal speed and

heading,  $P(\tilde{s})$  and  $P(\tilde{h})$ , the position of the vehicle in the ENU coordinate system can be predicted as follows.

$$\begin{aligned}\bar{x}(t_1) &= x(t_0) + \iiint_{t_0}^{t_1} \tilde{s} \cos(\tilde{h}) P(\tilde{s}) P(\tilde{h}) dt d\tilde{s} d\tilde{h}, \\ \bar{y}(t_1) &= y(t_0) + \iiint_{t_0}^{t_1} \tilde{s} \sin(\tilde{h}) P(\tilde{s}) P(\tilde{h}) dt d\tilde{s} d\tilde{h},\end{aligned}\quad (10)$$

Where  $t_1$  and  $t_0$  denote the time instance of prediction and last received BSM respectively. In this work, since the vehicles' states were measured every  $100ms$ , we calculated the predicted positions using the recursive piece-wise linear formulation.

$$\begin{aligned}\bar{x}(t_{j+1}) &= (t_{j+1} - t_j) \iint \tilde{s}_j \cos(\tilde{h}_j) P(\tilde{s}_j) P(\tilde{h}_j) d\tilde{s}_j d\tilde{h}_j \\ &\quad + \bar{x}(t_j) = \mathbb{E}[s_j] \mathbb{E}[\cos(h_j)] + \bar{x}(t_j) \\ &= \mu_{s_j} e^{-\sigma_{h_j}^2/2} \cos(\mu_{h_j}) + \bar{x}(t_j), \\ \bar{y}(t_{j+1}) &= (t_{j+1} - t_j) \iint \tilde{s}_j \sin(\tilde{h}_j) P(\tilde{s}_j) P(\tilde{h}_j) d\tilde{s}_j d\tilde{h}_j \\ &\quad + \bar{y}(t_j) = \mathbb{E}[s_j] \mathbb{E}[\sin(h_j)] + \bar{y}(t_j) \\ &= \mu_{s_j} e^{-\sigma_{h_j}^2/2} \sin(\mu_{h_j}) + \bar{y}(t_j)\end{aligned}\quad (11)$$

where,  $t_j - t_{j-1} = 100ms$  and  $t_0$  is the time instance of last received BSM.  $P(\tilde{s}_j)$  and  $\mu_{s_j}$  are the uni-variate predictive distribution of longitudinal speed at time instance  $t_j$  and its corresponding mean.  $P(\tilde{h}_j)$ ,  $\mu_{h_j}$ , and  $\sigma_{h_j}^2$  are the uni-variate predictive distribution of heading at time instance  $t_j$ , its corresponding mean, and variance. These values can be calculated using equation (9).

The pseudo-code of our model generation scheme is illustrated in Algorithm 1, in which  $PTE$  is the Position Tracking Error and is calculated as the 2D Euclidean distance between the actual and predicted vehicle positions. Since  $PTE$  sampling is dependent on the availability of actual position updates, it can be done at most at the sampling rate of GPS updates, which is 10 Hz for the SPMD dataset.

In the algorithm, the vehicles' states (speed,  $\mathcal{S}$  and heading,  $\mathcal{H}$ ) for all  $N$  available trips ( $T_i$ ,  $i = 1, \dots, N$ ) are loaded one after another. A kernel ( $K_i \in \mathcal{K}$ ) is selected and used to predict the time series at each time-step, the kernel  $K_i$  refers to the speed and heading kernels, the speed kernel is used to predict  $\mathcal{S}^*$  and the heading kernel to predict  $\mathcal{H}^*$ . When a kernel is selected, its prediction accuracy is evaluated at each time step ahead.  $HGP_{predict}$  is used to predict with the current kernel  $K_{current}$  from the bank of kernels. As long as the kernel predicts the future positions with a  $PTE$  less than the threshold ( $PTE_{th}$ ), it remains as the selected kernel for the model and keeps using this kernel until its prediction error exceeds the threshold ( $PTE > PTE_{th}$ ). The size of the time interval, in which the latest selected model remains in use, is called Model Persistency ( $MP$ ). At this moment either another kernel from the kernel bank is selected for predicting the position or, if none of the available kernels could satisfy the  $PTE_{th}$ , a new one is created and added to the bank  $\mathcal{K}$ ,

---

### Algorithm 1 Training: HGP kernel bank generation

---

```

1: Dataset: SPMD Trips  $\mathcal{T} = \{T_1, \dots, T_n\}$ ;  $i = 1$ 
2: Observe a TW history of  $\mathcal{S}^{obs}$  and  $\mathcal{H}^{obs}$ 
3: Fit first model  $K_{current} = HGP_{fit}(\mathcal{S}^{obs}, \mathcal{H}^{obs})$ 
4: for  $T_i \in \mathcal{T}$  do
5:   Read trip  $T_i$  load training  $\mathcal{S}$ ;  $\mathcal{H}$ 
6:   for  $t_{step} \in T_i$  do
7:     Use  $K_{current}$ 
8:     while ( $PTE < PTE_{th}$ ) do
9:        $\mathcal{S}^*, \mathcal{H}^* = HGP_{predict}(\mathcal{S}^{obs}, \mathcal{H}^{obs}, K_{current}, t_{predict})$ 
10:       $(X^*, Y^*) = XY_{predict}(\mathcal{S}^*, \mathcal{H}^*)$ 
11:       $PTE = f_{PTE}(X^*, Y^*)$ 
12:    end while
13:    for  $K_i \in \mathcal{K}$  do
14:       $\mathcal{S}^*, \mathcal{H}^* = HGP_{predict}(\mathcal{S}^{obs}, \mathcal{H}^{obs}, K_{current}, t_{predict})$ 
15:       $(X^*, Y^*) = XY_{predict}(\mathcal{S}^*, \mathcal{H}^*)$ 
16:       $PTE_{K_i} = f_{PTE}(X^*, Y^*)$ 
17:    end for
18:     $PTE_{min} = \min(PTE_{K_i})$ 
19:    if ( $PTE_{min} < PTE_{th}$ ) then
20:      Load kernel,  $K_{current} = \underset{K_i \in \mathcal{K}}{\operatorname{argmin}} PTE(K_i)$ 
21:    else
22:      Observe a TW history of  $\mathcal{S}^{obs}$  and  $\mathcal{H}^{obs}$ 
23:      Fit new model  $K_{current} = HGP_{fit}(\mathcal{S}^{obs}, \mathcal{H}^{obs})$ 
24:      Add  $K_{current}$  to  $\mathcal{K}$  bank
25:    end if
26:  end for
27: end for

```

---

$HGP_{fit}$  is used to learn the new model. Finally, we update  $K_{current}$  and continue the prediction with the updated kernel.

After the full kernel bank is created, the models are clustered to obtain a reduced-size kernel bank of vehicle behaviors, the limited-size kernel bank suffices to model the joint vehicle's dynamic and behavioral pattern of the driver. During forecasting, the model with the highest likelihood is chosen from the reduced kernel bank. Figure 5 shows a diagram of the training procedure explained before.

### B. Forecasting

Considering that the pre-learned reduced-size kernel bank is available at HV, every time the HV receives a new BSM from RV, it can choose a model from this kernel bank to forecast the trajectory (states) of the RV up until it receives the next BSM. For this purpose, assume that during the past  $T$  seconds, HV received BSMs from RV at time instances  $\mathbf{t}$  and the value of speed and heading of the RV at these time instances (from received BSMs) are denoted by  $\mathcal{S}$  and  $\mathcal{H}$ . The best model from the bank, with the highest likelihood, is selected by using the following equation.

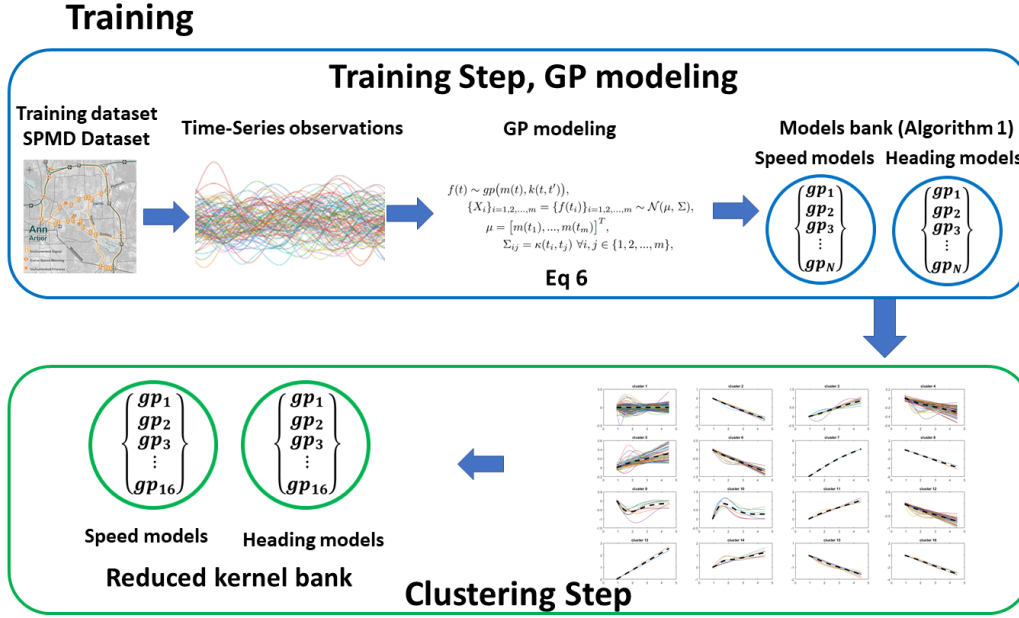


Fig. 5: Offline training and clustering.

$$\begin{aligned}
 \theta_s^* &= \underset{\theta_s \in \text{speed bank}}{\operatorname{argmax}} \log p(\theta_s | \mathcal{S}, \mathbf{t}) = -\frac{n}{2} \log 2\pi \\
 &\quad - \frac{1}{2} \mathcal{S}^T K_S^{-1}[(\mathbf{t}, \mathbf{t}) | \theta_s] \mathcal{S} - \frac{1}{2} \log \det(K_S[(\mathbf{t}, \mathbf{t}) | \theta_s]) \\
 \theta_h^* &= \underset{\theta_h \in \text{heading bank}}{\operatorname{argmax}} \log p(\theta_h | \mathcal{H}, \mathbf{t}) = -\frac{n}{2} \log 2\pi \\
 &\quad - \frac{1}{2} \mathcal{H}^T K_H^{-1}[(\mathbf{t}, \mathbf{t}) | \theta_h] \mathcal{H} - \frac{1}{2} \log \det(K_H[(\mathbf{t}, \mathbf{t}) | \theta_h])
 \end{aligned} \tag{12}$$

Where  $\theta_s$  and  $\theta_h$  are the hyperparameters of the speed and heading models in the bank,  $n$  is the size of vector  $\mathbf{t}$  and  $K_S$  and  $K_h$  are the covariance matrix of speed and heading observations given hyperparameters  $\theta_s$  and  $\theta_h$  and can be constructed using equation (5).  $\theta_s^*$  and  $\theta_h^*$  are hyperparameters of the selected speed and heading models with the highest likelihood. Using the selected model, we can predict the future values of speed and heading and consequently predict the position by utilizing (9) and (11).

Figure 6 depicts how the final prediction is obtained from the history of time-series observations. After the prediction model is selected, speed and heading are predicted and used to predict  $X$  and  $Y$  and the final path. When packets are not received, the time series history is used to select the corresponding model. If there is no model in the reduced kernel bank that meets the required  $PTE_{th}$  a new model is created, added to the bank, and selected for prediction. Next, the selected model is used for forecasting the RV's states and keeping track of the RVs even when the data is not received.

GP predictions are swapped with constant speed and constant acceleration predictions if a specific criterion is met

for avoiding divergence of speed and acceleration predictions to infinity or to unfeasible values when the time interval between two consecutive BSMs is large and we must rely on prediction for a long period. Figure 7 shows the diagram for the hybrid prediction procedure. Different motion models are used based on physical constraints in order to increase the accuracy and robustness of the prediction. This hybrid procedure proves to be advantageous, especially in situations where the assumptions of the other models are no longer valid. For visualization, the results of the hybrid approach against constant acceleration on a single trip are shown in Figure 8.

## V. EXPERIMENTAL SETUP AND SIMULATION RESULTS

We study the impact of communication uncertainties on the proposed CA-TC and compare it with the other architectures, demonstrating that the proposed prediction system outperforms the baselines.

### A. Data Preprocessing

We evaluate three separate datasets to validate the proposed architecture. To begin, we replicate realistic scenarios using SUMO simulation data. Then we use the 100-car dataset [54] and lastly, we evaluate our approach using the SPMD dataset. **SUMO Dataset.** We first evaluate our approach using the created SUMO dataset. We generate logs that contained information such as timestamps, vehicle IDs, GPS coordinates, and velocities and create the BSM packets for different timestamps based on the standard BSM transmission frequency (i.e. 10Hz). SUMO enables the testing of any real-world road scenario without the need for costly and time-consuming real-world data collecting. The designed scenarios are carefully chosen from OpenStreetMap and exported into the SUMO simulator,

## Forecasting

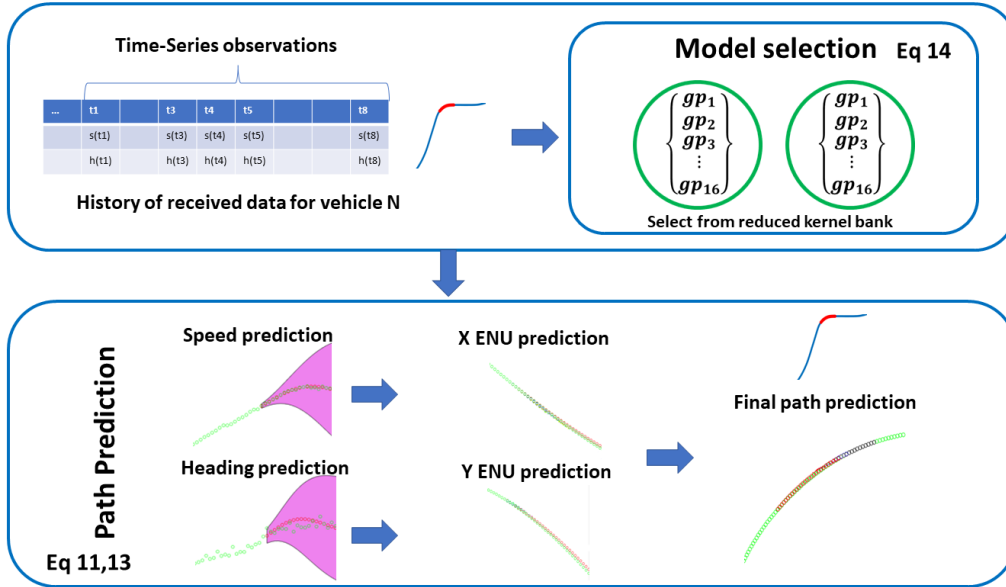


Fig. 6: Path prediction example using HGP.

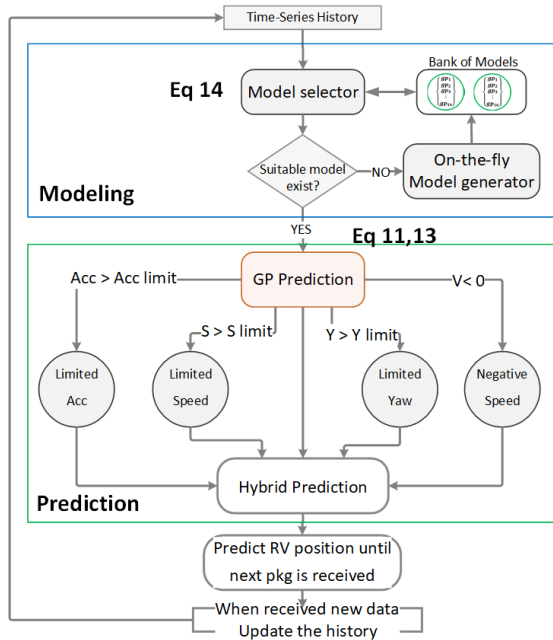


Fig. 7: On-the-fly model Forecasting Diagram.

where we construct situations with the required vehicle density and behavior, and then utilize the intended scenarios to evaluate the performance of our system and CVS applications.

**100-Car Dataset.** We utilize the Virginia Tech Database dataset (100-car dataset). This dataset contains trajectories for over 800 real-world instances, some of which are near-crash or real crashes. The data is utilized to build a lead vehicle (RV) and a following vehicle (HV) movement using a car-

following model as described in [55]. The subsequent vehicle mobility is used to evaluate the system's performance. As a consequence, we have trajectories for two cars (one RV and one HV), with the RV trajectories being based on real data and the HV trajectories being generated using the car-following model.

**SPMD Dataset.** Finally, we evaluate the performance of our system using the SPMD [52], which is a well-known data set that contains a wide range of trips recorded on various metropolitan roads by various sorts of cars and drivers. SPMD is a comprehensive data collection that reflects a wide variety of driver/vehicle actions and movements. The SPMD dataset provides various in-car data logged through CAN, such as longitudinal velocity and acceleration, yaw rate, steering angle, turning signal status, etc., as well as vehicle GPS data for the duration of the complete trip duration. To encourage the selection of a diverse set of trajectories, all the trips from the SPMD dataset are first ranked based on the experimental criteria and then 50 of the richest and most diverse trips are chosen. All trips are ranked on the merits of trip duration, number of successful lane changes, number of aborted lane changes, number of times a vehicle used a turning signal in a trip, number of times a vehicle stopped in a trip, and standard deviation of vehicles' yaw rate, steering angle, GPS heading and longitudinal acceleration. These 50 richest trips, which include more than 300,000 sample points, are plotted, and visually inspected to confirm the proper selection.

The logs from the datasets (SUMO, 100Car, and SPMD) are used to recreate different communication scenarios. The logs are transferred to an OBU, replayed, and transmitted over the air by using the RVE that we have developed jointly in collaboration with industry partners for this purpose [9].

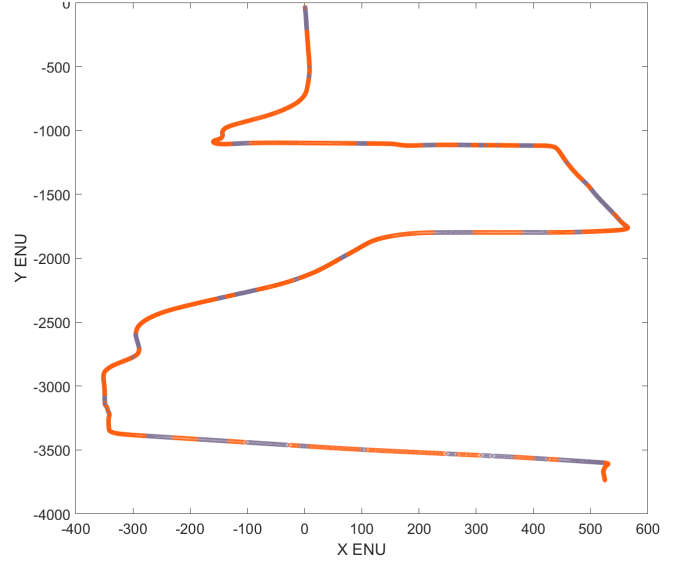
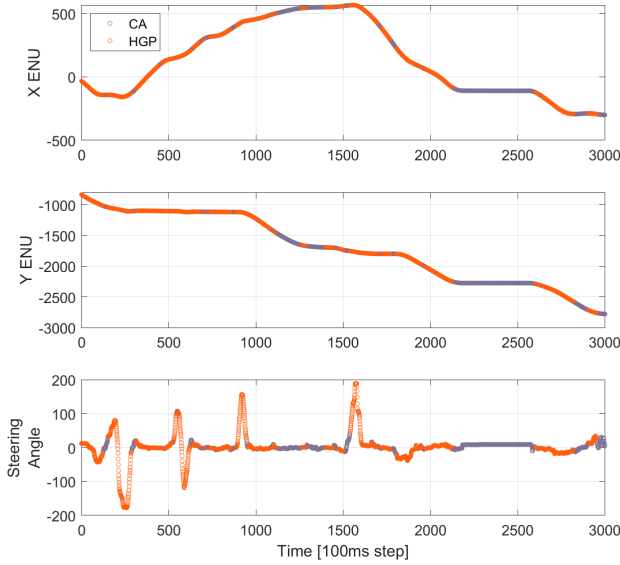


Fig. 8: Performance of our HGP scheme against constant acceleration (CA). The figure (using different colors) shows the moments when CA over-performs HGP (in terms of  $PTE$ ) on the tracking accuracy while remaining below the threshold. (left) shows the performance by timesteps, (right) shows the performance in 2D ENU coordinates.

By leveraging hardware-in-the-loop, the RVE allows the joint study of CVS applications and their underlying communication system in real-time. As such, it serves the important purpose of validating the designed architecture.

### B. Prediction Baseline Models

In order to evaluate the performance of the Hybrid GP prediction and demonstrate the capabilities of the architecture, different prediction schemes are implemented. As a baseline, we compare **BSM-dependent** (No estimation), prediction with Constant Speed (**CS**), Constant Acceleration (**CA**), Kalman Filter (**KF**), Auto Encoder (**AE**), Long short-term memory (**LSTM**), and the proposed hybrid GP-based scheme (**HGP**). In the next section, we describe the tested baselines.

For AE, LSTM and GP prediction, the  $(x, y)$  predictions can be obtained following two different approach, i.e. direct (**D**) or indirect (**I**). In the direct approach,  $(x, y)$  are treated as two independent time series, and the history of  $(x, y)$  is used to learn models for  $(x, y)$ , producing direct predictions of futures  $(x, y)$ . Differently, in an indirect approach, the heading and longitudinal speed of the vehicle are treated as two independent time series and the history of heading and longitudinal speed are used to learn models to forecast the vehicles' speed and heading. The predicted heading and speed are used to indirectly predict the future position  $(x, y)$ . In our experiments, when we refer to AE, LSTM, and HGP, the indirect approach is used. When the direct approach is used we a referred to as AE-D, LSTM-D, and HGP-D.

1) *Kinematic Models*: The BSM-dependent design (i.e. no prediction) keeps the last received position acquired from the BSM of that RV until the HV receives a new BSM from that RV. Although it is simple to implement and reduce the

computation complexity of the system, it is not a realistic assumption and can lead to huge  $PTE$  and the consequent drastic reduction in the performance of safety applications. The time update equation is  $X(t+1) = X(t)$ , where  $X(t)$  is the position of vehicle at time  $t$ .

In the CS scheme, we assume that the vehicles' speed will remain unchanged during each inter-packet gap (IPG). The algorithm uses the speed from RV's last received BSM until it receives the next packet. This assumption is reasonable when the IPG is small and the HV is receiving BSMs at regular intervals. The time update equations are as below.

$$X(n) = \begin{bmatrix} x(n) \\ s(n) \\ a(n) \end{bmatrix} \quad (13)$$

$$X(n+1) = \begin{bmatrix} 1 & T_s & 0 \\ 0 & 1 & 0 \\ 0 & 0 & 0 \end{bmatrix} X(n) \quad (14)$$

Where  $X(t)$  is the vector of vehicle states at time  $t$  and  $T_s$  is the sampling time. This experiment assumes that  $T_s = 100ms$ , which is the standard message transmission rate according to the IEEE J2735 standard. In an event of the reception of a new packet, the measurement update takes place.

The CA scheme is similar to the former approach, except that we assume acceleration to remain constant during the IPG duration. The time update mechanism follows the equation below:

$$X(n+1) = \begin{bmatrix} 1 & T_s & \frac{T_s^2}{2} \\ 0 & 1 & T_s \\ 0 & 0 & 1 \end{bmatrix} X(n) \quad (15)$$

2) *Kalman Filter Model*: The KF is essentially a set of mathematical equations that implement a predictor-corrector type estimator that is optimal in the sense that it minimizes the estimated error covariance when some presumed conditions are met. Rarely do the conditions necessary for optimality actually exist, and yet the filter works well for many applications. The KF addresses the general problem of trying to estimate the state of a discrete-time controlled process, it assumes that the state at time  $k$  evolves from state  $k - 1$  according to the state update equation as,

$$X_k = AX_{k-1} + Bu_{k-1} + w_{k-1} \quad (16)$$

And at time  $k$  a measurement(observation) is made according to,

$$y_k = H_k X_k + v_k \quad (17)$$

Where  $X$  and  $y$  represent the state vector and measurement vector;  $w_k$  and  $v_k$  represent the process and measurement noise respectively. The process and measurement noises are assumed to be independent white noises with normal probability distribution with covariances  $Q_k$  and  $R_k$  respectively. The matrix  $A$  ( $n \times n$ ) is the state transition matrix which is applied to the previous state  $X_{k-1}$ , the matrix  $B$  ( $n \times 1$ ) is the control input matrix which is applied to the control vector  $u_k$ , and the matrix  $H$  ( $m \times n$ ) is the observation model, which maps the state space into the observed space, it relates the state  $X_k$  to the measurement  $y_k$ .

The KF computation is divided into two parts: time update and measurement update. The time update is responsible for projecting forward the current state and error covariance estimates in time to obtain a priori estimates for the next time step. The measurement update is responsible for incorporating a new measurement into a priori estimate to obtain an improved posteriori estimate. The final prediction algorithm resembles that of a predictor-corrector algorithm. The time and measurement equations are as below:

Time update equations:

$$X_k = AX_{k-1} + Bu_{k-1} + w_{k-1} \quad (18)$$

$$P_k = AP_{k-1}A^T + Q \quad (19)$$

Measurement update:

$$K_k = P_k H^T (H P_k H^T + R)^{-1} \quad (20)$$

$$X_k = X_k + K_k (y_k - H X_k) \quad (21)$$

$$P_k = (I - K_k H) P_k \quad (22)$$

Particularly, as a baseline, we consider a Kalman Filter with a constant acceleration dynamic, and describe the state transition equations as follows,

$$X_k = \begin{bmatrix} x_k \\ s_k \\ a_k \end{bmatrix} \quad (23)$$

$$\hat{X}_k = \begin{bmatrix} 1 & T_s & \frac{T_s^2}{2} \\ 0 & 1 & T_s \\ 0 & 0 & 1 \end{bmatrix} \hat{X}_{k-1} + w_{k-1} \quad (24)$$

$$y_k = [1 \quad 1 \quad 1] \hat{X}_k + v_k \quad (25)$$

When a new packet is received, both measurement and time updates are running, and when a packet loss happens the prediction is done based on only the time update. Based on a statistical analysis of the dataset the variance of the measurement noise, the  $R$  matrix, is specified as,

$$R = \begin{bmatrix} 10 & 0 & 0 \\ 0 & 1 & 0 \\ 0 & 0 & 0.5 \end{bmatrix}$$

3) *Autoencoder Model*: Neural network architectures such as AE use unsupervised learning or self-supervised learning. The AE architecture can vary, but in general it consists of an encoder, which reduces the input's dimension, it maps the input  $x$  to a latent feature representation  $z$  denoted by  $z = f_{w_e}(x)$ , and a decoder, which attempts to recreate the original input from the lower-dimensional representation, using the latent representation  $z$  to obtain a reconstruction  $y$  of the input  $x$ , denoted by  $y = f_{w_d}(z)$ . The goal of training these algorithms is to be able to recreate the original input with the fewest information losses possible, by minimizing the reconstruction error between  $x$  and  $y$ . As a generative model, an AE can be trained for a prediction task using a similar methodology, by training the AE to reproduce the state at time  $t + 1$  given the state at time  $t$ . In our baseline, we design an encoder that consists of 3 fully connected (FC) layers with 256, 128, and 64 units respectively. The encoder takes as input the time-series observations and outputs the internal representation that is passed to the decoder, the decoder consists of a symmetric version of the encoder. For multiple-step predictions, the predictions are used in a chain to generate subsequent predictions.

4) *LSTM Model*: An LSTM is a kind of Recurrent Neural Network. LSTMs are particularly helpful when using time series or sequential data due to their capacity to learn long-term dependencies. The LSTM network is able to learn a function that maps the time series history to feature predictions. For the LSTM baseline in this paper, we use a model similar to [41] with two layers of 256 LSTM cells, ReLu activation, and dropout. The model is fit using Adam and MSE loss function. It is mainly a regression problem solved by the LSTM model with the goal to predict future positions  $(x, y)$  for the neighboring vehicles.

### C. Controlled Variables

We conducted a set of experiments to measure the performance of our architecture and investigate the existence of a reduced kernel bank size that is capable of accurately modeling driving behaviors. Then, the feasibility of the real-time implementation of the proposed system is also analyzed in terms of computation time. Finally, the overall system performance is

evaluated against the previous baselines. For that purpose, we choose appropriate controlled variables, i.e, Training Window (**TW**), which is defined as the number of the latest equally spaced received samples (e.g., most recent history of heading and speed time series) utilized as the training data to generate each model, Cluster Size (**C<sub>size</sub>**), Packet Error Rate (**PER**) and Transmission Rate (**Rate**). We investigate how the *TW* and *C<sub>size</sub>* affect the model performance. Finally, In order to study the impact of communication losses, we use *PER* and *Rate* and measure the performance of the different prediction schemes and safety applications under different *PER* and *Rate*. When measuring the impact of *PER*, the *Rate* is fixed to 10Hz and when measuring the impact of *Rate*, the *PER* is fixed to 0%.

#### D. Performance Metrics

To assess the influence of the controlled variables we select suitable performance metrics, i.e, Model Persistency (**MP**), computation time (**t<sub>c</sub>**), Warning Accuracy (**WA**) and Position Tracking Error (**PTE**). In order to gauge the impact of *TW*, we study how *MP* and *t<sub>c</sub>* change with *TW* size. We evaluate the influence of the *C<sub>size</sub>* by measuring the performance of the system in terms of *MP* for different *C<sub>size</sub>*. Finally, to measure the overall system performance, we select two performance metrics, *WA* and *PTE*, that while correlated, provide different insights into the advantages of our approach. *PTE* is more related to the quantitative estimation performance and *WA* is related to the performance of the safety applications. *WA* and *PTE* have been used successfully as good indicators of the performance of the CVS applications [11], [12].

**Position Tracking Error (PTE).** In all the experiments, *PTE* describes the 95th percentiles of the error in tracking the position of RV. While it measures the quantitative performance of the prediction method, it isn't the best indicator of the application performance. For this purpose, we use *WA*, which indicates how well the safety application is performing.

**Warning Accuracy (WA).** For the purpose of validation in this paper, we focus on the FCW application, and we study the impact of communication losses on FCW accuracy (*FCW<sub>accuracy</sub>*). While there are many different implementations of FCW, we use the CAMP Linear FCW algorithm [17], [24]. The used CAMP Linear FCW algorithm is briefly described in the next section. In that sense, the warnings are based on the CAMP Linear algorithm and ground truth data is the output of the CAMP Linear algorithm when *PER*=0 % and *Rate*=10Hz. For *FCW<sub>accuracy</sub>*, we compare the ground truth and FCW application output for different values of *PER* and *Rates* while different prediction schemes are used. More precisely, *FCW<sub>accuracy</sub>* is the ratio of true negatives plus true positives across all execution instances and is defined as follows:

$$FCW_{accuracy} = \frac{T_p + T_n}{F_p + F_n + T_p + T_n} \quad (26)$$

where  $T_p$  (True positive) and  $T_n$  (True negative) are the numbers of correctly predicted hazards and safe indications;

$F_n$  (False negative) is the number of incorrectly predicted safe indications (misidentified actual hazards), and  $F_p$  (False positive) is the number of incorrectly predicted hazard indications (misidentified actual safe situations).

We compare the *PTE* and *FCW<sub>accuracy</sub>* (Performance metrics) of the CA-TC-based architecture using different prediction schemes, while *PER* and *Rate* (Controlled variables) change from 0 to 95 % and from 10Hz to 1Hz respectively.

Although our architecture is agnostic to the V2X communication technology, in our setup, we used the V2X device (DSRC-based) DENSO WSU-5900A and the RVE to evaluate the performance of the system [9]. We show the results of the analyses for the SUMO, 100-Car, and SPMD datasets by using the mobility logs together with the RVE. The RVE can imitate network congestion scenarios with different *PER* or *Rates*.

#### E. Cooperative Forward Collision Warning (FCW)

In this section, we briefly present the FCW CAMP Linear algorithm implementation used in the experiments [17], [24]. FCW algorithms are intended to notify the driver when the present movement pattern of cars indicates that a collision is imminent. The warning should be timed such that it takes into account the driver's reaction time, but not so quickly that it causes false alarms. FCW is run repeatedly (e.g., 100 ms intervals) and at each interval is evaluated if a threat exists. The FCW CAMP Linear algorithm evaluates a "warning range" ( $r_w$ ) using RV and HV data. A warning is issued if the distance between the HV and the RV is less than the  $r_w$  [11], [17], [24].

**CAMP Linear FCW algorithm.** In the CAMP Linear FCW algorithm, the  $r_w$  is computed as:

$$r_w = BOR + (v_{HV} - v_{RV})t_d + \frac{1}{2} * (a_{HV} - a_{RV})t_d^2 \quad (27)$$

Where  $r_w$  is the warning range, *BOR* is the Brake Onset Range;  $v_{HV}, v_{RV}, a_{HV}, a_{RV}$  are the speed and acceleration of HV and RV and  $t_d$  is the driver and brake system reaction delay. The *BOR* is computed for three different scenarios, for stationary or moving RV, as follows.

- **Case 1:** RV stationary.
- **Case 2:** RV moving at the beginning and end of the scenario.
- **Case 3:** RV moving at the beginning but stopping at the end of the scenario.

$$\begin{aligned} \text{Case 1: } BOR &= \frac{v_{HVp}^2}{-2 * a_{req}} \\ \text{Case 2: } BOR &= \frac{(v_{HVp} - v_{RVp})^2}{-2 * (a_{req} - a_{RV})} \\ \text{Case 3: } BOR &= \frac{v_{HVp}^2}{-2 * a_{req}} - \frac{v_{RVp}^2}{-2 * a_{RV}} \end{aligned} \quad (28)$$

in witch,  $v_{HVp}$  and  $v_{RVp}$  are the predicted velocity of HV and RV, i.e,  $v_{HVp} = v_{HV} + a_{HV}t_d$  and  $v_{RVp} = v_{RV} + a_{RV}t_d$ .  $a_{RV}$  is the acceleration (deceleration) of RV and  $a_{req}$  is the deceleration that is required at the HV for avoiding a crash and is modeled in [24] using real data.

## F. Hypotheses

Based on the defined **controlled variables** and **performance metrics** we examine the following hypotheses:

- **H1.** An suitable **TW** needs to be selected in order to allow an acceptable model persistency (**MP**) and meet the real-time requirements of the CVS applications measured by computation time ( $t_c$ ).
- **H2.** We anticipate the existence of a limited size of kernel banks ( $C_{size}$ ) which is capable of predicting driving behavior while keeping an acceptable **MP** horizon. The kernel bank can be learned offline and still be useful during on-the-fly forecasting.
- **H3.** The higher the **PER** or the lower the **Rate of communication**, the greater the impact and benefit of using our CA-TC system, measured by **PTE** and **FCW<sub>accuracy</sub>**. Thus, we expect a higher **FCW<sub>accuracy</sub>** when using our HGP prediction scheme when compared to the baselines.

The hypotheses are investigated through the experiments in the following sections.

## G. GP Prediction Model Hyper Parameter Tuning and Implementation Details

As described, in the Hybrid GP modeling scheme instead of working directly on the X-ENU and Y-ENU time series, the heading, and speed of the vehicle are treated as two independent time series. The GP models, which are learned from speed and heading histories are used to forecast their future value, and then the predicted values of these two variables are used to predict the position in ENU coordinate system. In this section, we present the study of **TW** and  $C_{size}$  and obtain suitable values for those variables to be used for the HGP prediction system.

1) *Computational Complexity:* To study the hypothesis **H1** we investigate the effect **TW** in computation time and experimentally compute the computation time of our algorithm for **TW** size from 1 to 1000. The HGP training (new kernel generation) and forecasting complexity is a function of the training window. In our framework, this factor appears whenever we need to generate a new kernel while we are running the system in real-time. The order of this complexity is heavily dependent on the implementation strategy of GP kernel training algorithms. In the simulations, we have used the "Gaussian Process for Machine Learning" MATLAB toolbox, provided by Cambridge University.

Figure 9 shows the result of the experimental estimation, in the right plot the blue curve shows the actual spent time and the red one is the quadratic approximations, as shown for a large number of training windows, the complexity of our algorithm is quadratic ( $O(n^2)$ ). The Root Mean Square Error (RMSE) values for the fitted curve are also presented in the figure. In the left plot, a plot of the computation time for training windows size up to 60 is presented. As shown we can train up to **TW** size 40 and still be under the 100ms threshold required for safety applications. The simulations have been

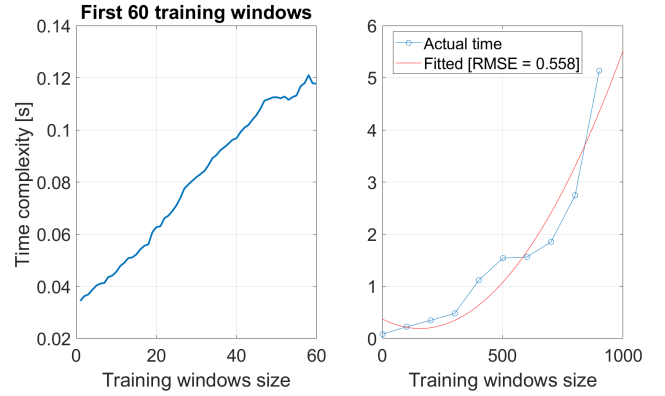


Fig. 9: Empirical time complexity of GP kernel training as a function of training window size.

executed on a PC with an Intel Core i7 6700 3.4 GHz CPU with 4 cores and 32 GB of RAM. The results in Figure 9 validate the **H1** and allows us to select a suitable **TW** that meets the real-time requirements of the CVS applications. Additionally, we want to mention that our approach can benefit from parallel computing during the bank kernel creation and during forecasting, as the model predictions can be computed independently in parallel, therefore the use of GPU or a CPU with additional cores will further reduce the computation time. Based on our experiments and previous work [51], we choose a **TW** size of 30 time-steps (3s) and  $PTE_{th} = 50cm$  for the training, model generation, and forecasting. The selected training parameters consider an acceptable path history while also meeting the computational requirement of the safety applications.

2) *Model Generation:* To examine the hypothesis **H2**, we obtain the kernel bank and experiment with different cluster sizes. Following the HGP training and model generation schemes in Algorithm 1, we obtained 350 models, and reduce the kernel bank by clustering the kernels. For each  $C_{size}$  we compute the model persistency (**MP**) when predicting future trajectories while keeping the error within the defined  $PTE_{th}$ . Figure 10 shows how **MP** changes for different  $C_{size}$ . The results support the hypothesis **H2** and confirm the existence of a reduced-size kernel bank capable of predicting driving behavior patterns. From those results, we choose a cluster size of 16 that has a reduced size while keeping an adequate **MP**, balancing complexity and performance. Therefore the models from the original kernel bank are clustered in the 16 most distinctive models to form the reduced kernel bank.

During on-the-fly mode, the most recent information is used to learn the parameters of the Gaussian process's Kernel. In the experiments, we use BSMs received during the last **TW** to learn the new model. This model will be used to forecast the state of the vehicle until new information is received or the forecasted speed or acceleration of the vehicle triggers the model switching based on the algorithm described in Figure 7.

Finally, to test the capability of the reduced kernel bank, we apply the trained kernel bank to a new set of 50 randomly

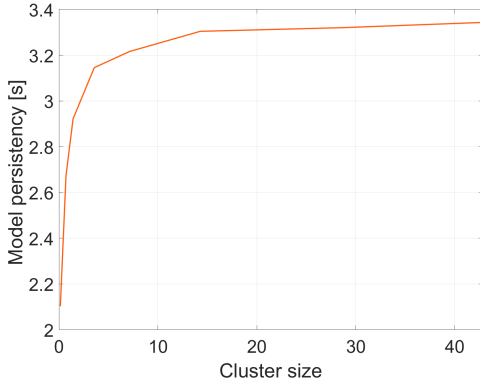


Fig. 10: Model persistency for different cluster sizes.

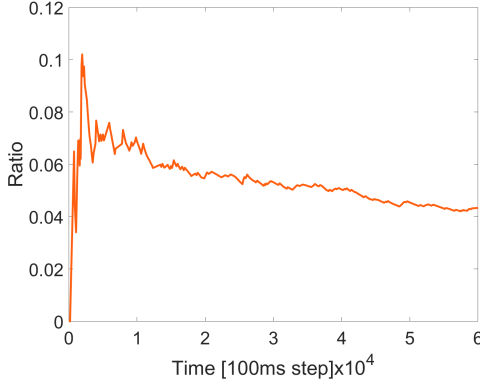


Fig. 11: Assessment of trained kernel bank performance in terms of required new kernel generation rate for an unforeseen set of trajectories.

selected trajectories. Therefore, they could be considered as a set of generic driving data. The ratio of generating new models, which has been represented in Figure 11, has an increasing trend at the beginning of test time and raises to around 10% at its maximum level, and then it converges around 4%. This observation shows that the learned kernel bank is meaningful during the testing phase (on-the-fly forecasting), even for unforeseen data, further verifying the hypothesis **H2**.

#### H. Overall system performance

Finally, to investigate the **H3**, we use the parameters obtained for our HGP prediction system, i.e.  $TW = 3s$ ,  $PTE_{th} = 50cm$ , and  $C_{size} = 16$ , and study the impact of communication uncertainties on the performance of a selected safety application with proposed CA-TC and compare it with the baselines across multiple datasets.

**Experiments with SUMO simulated data** We first use the data generated from the SUMO simulator and compare the baseline models against our approach. Figure 12 demonstrates  $FCW_{accuracy}$  and  $PTE$  for different values of  $PER$  and  $Rates$  using the SUMO data. As expected, the  $FCW_{accuracy}$  of the BSM-dependent baseline is the lowest, and the  $PTE$  is the highest. For the SUMO simulated data, the KF model

and GP perform similarly which could be a consequence of the simplistic car-following model utilized in SUMO.

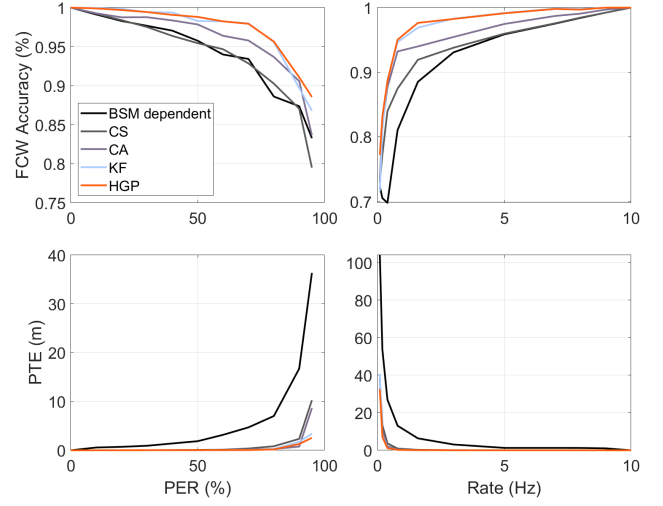


Fig. 12:  $PTE$  and  $FCW_{accuracy}$  vs  $PER$  and  $Rate$  for the SUMO dataset.

**Experiments with the 100-Car Dataset** We also evaluated the performances using the 100-Car dataset. Figure 13 shows how the  $PTE$  and  $FCW_{accuracy}$  change for the different  $PER$  and  $Rate$  values. Similarly, the BSM-dependent model shows the highest  $PTE$  and lowest  $FCW_{accuracy}$ . HGP has a similar performance to KF or CA models. We speculate that the reason for having similar performances is the car-following model used to create the HV states in the 100-Car dataset.

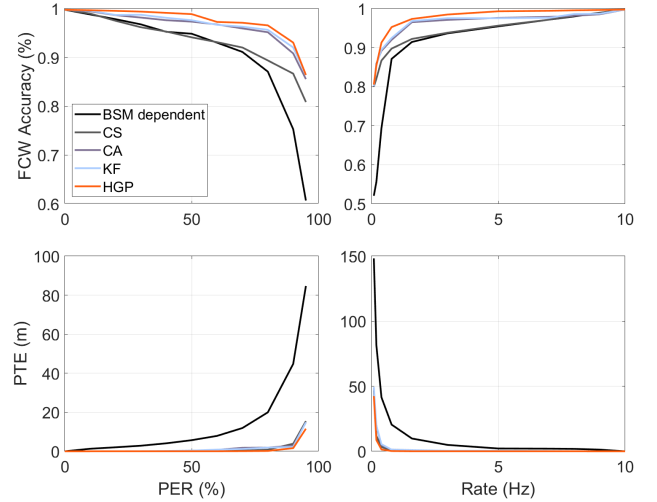


Fig. 13:  $PTE$  and  $FCW_{accuracy}$  vs  $PER$  and  $Rate$  for the 100-Car dataset

**Experiments with the SPMD dataset** Finally, using SPMD dataset [52], we compare the proposed HGP method with the baselines CA, KF, AE, and LSTM. We want to mention that the AE and LSTM models require a larger amount of data and

are not suitable for the SUMO and 100-Car datasets. Figure 14 shows the performance of all the models in the SPMD dataset. As expected, the KF model performed similarly to the CA model due to the chosen kinematic equation to model the vehicle motion in the KF method. However, the slight over-performance of KF is due to its ability to reduce measurement noise, in particular, the AE model shows poor performance for vehicle trajectory prediction. As  $PER$  increases over 60%, the HGP approach shows its superior prediction, as it can forecast for longer prediction horizons, and capture both the dynamics of the vehicle and the driver’s behavior. The difference in position tracking is notable as  $PER$  reaches 90%. The CA and KF approaches had 60% larger  $PTE$  compared to HGP. The LSTM model has a similar performance to our HGP model however LSTM models are data-hungry models and are not suitable for online on-the-fly training while new data is available, making it difficult to extract new knowledge from new situations, differently from the HGP approach that can learn new models on the fly, with a limited amount of data. The results demonstrate the superiority of our HGP approach and the benefits as  $PER$  increases, confirming the hypothesis **H3**.

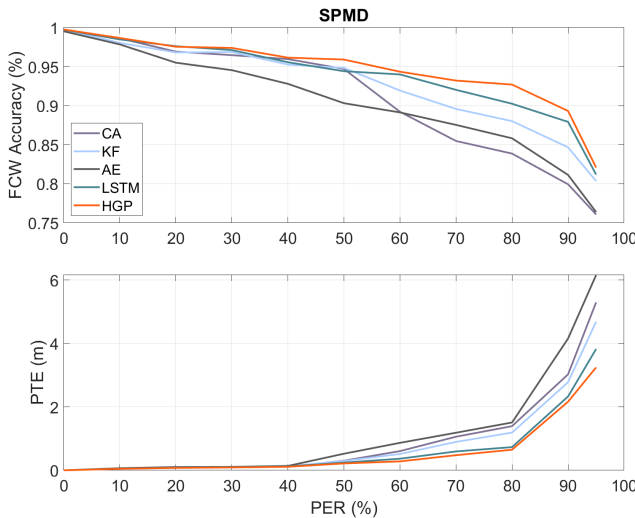


Fig. 14: Comparison of CA, KF, AE, LSTM and our HGP approach performance in the SPMD dataset, measured by  $FCW_{accuracy}$  and  $PTE$

Following in Table I we present the tabular results for the performance of the baselines and our HGP approach in the SPMD dataset, measured by the  $PTE$  at different  $PER$  values. For completeness, we include both direct (AE-D, LSTM-D, HGP-D) and indirect (AE, LSTM, HGP) approaches. The baseline methods are CA, KF, AE-D, LSTM-D, HGP-D, AE, LSTM, and HGP. The results from Table I show the improved performance when using the HGP in terms of  $PTE$ , which are more noticeable as communication losses increase measured by  $PER$ , verifying our **H3**.

We perform a sensitivity analysis and compare the performance of CA, KF, AE, and LSTM against the proposed

method based on  $PTE$  and the number of times in which a specific  $PTE$  threshold ( $PTE_{th}$ ) has been exceeded. We investigate different  $PTE_{th}$ s, i.e. from 0.2 m to 1.6m. In general, vehicular safety applications are sensitive to position-tracking error in a hard-thresholding manner. The value of this threshold is dependent on the application and the driving scenario. The position error exceeding the  $PTE_{th}$  can cause false positives and negatives in the safety applications and directly influence their performances.

In this test, in the case of a packet loss, the HV performs prediction and if the prediction error is larger than the threshold, it is counted as an inadmissible prediction, possibly causing a hazardous situation ( $PTE$  higher than the admissible threshold  $PTE_{th}$ ). In Figure 15, the total number of inadmissible predictions during the trajectories for different  $PTE_{th}$ s are plotted. For example, the plot in the top left shows the number of times that the  $PTE$  is bigger than  $PTE_{th} = 0.2m$ , which gives a sense of how many times an application that requires a  $PTE$  less than  $PTE_{th} = 0.2m$  will fail. The bottom right shows the number of times that the  $PTE$  is larger than  $PTE_{th} = 1.6m$  for different  $PER$ s. It shows that for a low  $PER$  the  $PTE$  never exceeds 1.6m, and for higher values of  $PER$ , the HGP performs better in all the cases. For instance, at  $PER = 90\%$  and  $PTE_{th} = 1.6m$ , CA fails more than 200% times compared to the proposed HGP, similarly, the proposed HGP outperforms the other baselines. These results confirm the notable superiority of our approach as  $PER$  increases and further validate hypothesis **H3**.

## VI. CONCLUSION AND FUTURE WORK

In this study, we proposed a Context-Aware Target Classification module with a hybrid Gaussian Process regression as the prediction module to improve the robustness and flexibility of CVS systems. Unlike previous works that are strictly information message dependent, the proposed CA-TC allows safety applications to work based on the context-aware map rather than individual information messages, alleviating the effect of information loss on the performance of safety applications. The HGP relies on a reduced-size bank of driving models learned offline from real data to perform forecasting on-the-fly, while also allowing the online adding of new driving models to the bank, accounting for unforeseen driving behaviors. We studied the impact of communication uncertainties, in terms of  $PER$  and  $Rate$ , on the performance of the safety applications using the proposed CA-TC and compare it to the baseline. The performance is measured both in terms of  $PTE$  and  $WA$ . The architecture is validated by simulation and real driving scenarios using three different datasets and a RV emulator based on a DSRC WSU. A notable performance improvement is observed using the proposed framework against traditional approaches.

**Limitations and Future Work.** While we proposed a novel prediction method to be used in our architecture, the CA-TC can be further improved by the integration of other prediction methods. Data fusion and cooperative perceptions are among

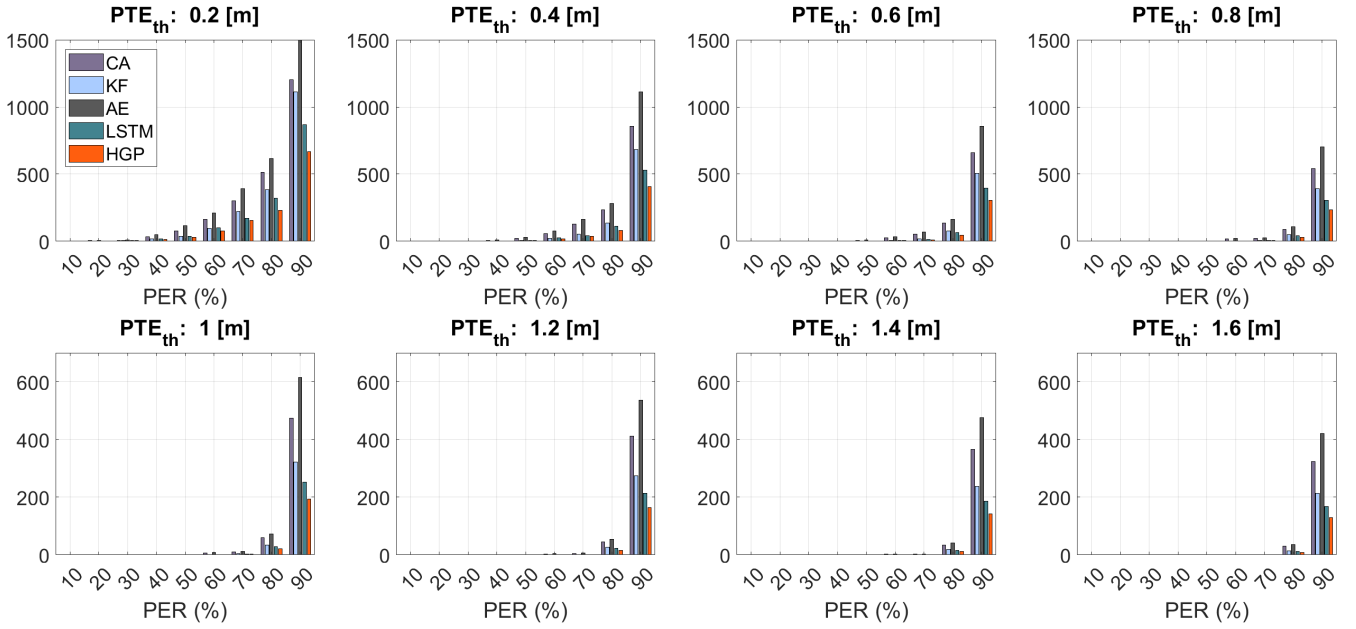


Fig. 15: Number of time which  $PTE$  threshold has been exceeded vs  $PER$  for different values of threshold ( $PTE_{th}$ )

TABLE I: Tabular results for the performance of the baselines and our HGP approach in the SPMD dataset, measured by the  $PTE[m]$  at different  $PER[\%]$  values. For both direct (AE-D, LSTM-D, HGP-D) and indirect (AE, LSTM, HGP) approaches.

Methods	PER [%]										
	0	10	20	30	40	50	60	70	80	90	95
CA	0.000	0.047	0.077	0.091	0.110	0.303	0.605	1.059	1.392	3.026	5.296
KF	0.000	0.059	0.093	0.098	0.126	0.293	0.514	0.895	1.189	2.778	4.687
AE-D	0.000	0.127	0.322	0.541	0.774	1.154	1.813	2.200	2.640	5.926	9.558
LSTM-D	0.000	0.110	0.292	0.356	0.559	0.683	0.865	1.417	1.781	4.231	6.918
HGP-D	0.000	0.108	0.299	0.322	0.413	0.546	0.824	1.106	1.599	4.167	6.473
AE	0.000	0.065	0.103	0.108	0.138	0.523	0.866	1.185	1.508	4.156	6.156
LSTM	0.000	0.051	0.085	0.100	0.122	0.243	0.366	0.595	0.731	2.329	3.825
HGP	0.000	0.047	0.076	0.089	0.111	0.216	0.281	0.476	0.649	2.163	3.245

the possible methods to be incorporated with the flexible CA-TC architecture to further enhance the safety application's performance. In future works, we will examine the integration of error-driven model-based communication into our system. We plan to investigate the existence of natural and meaningful driving patterns for long-term maneuver and driver's intention prediction. We also plan to experiment with more CVS applications and other baselines. In a parallel research direction, we plan to extend our work to non-cooperative applications and test our predictive model in different tasks from commonly used driving datasets such as KITTI and Waymo, among others.

## REFERENCES

- [1] Pengyuan Zhou, Pranvera Kortoçi, Yui-Pan Yau, Benjamin Finley, Xiujun Wang, Tristan Braud, Lik-Hang Lee, Sasu Tarkoma, Jussi Kangasharju, and Pan Hui. Aicp: Augmented informative cooperative perception. *IEEE Transactions on Intelligent Transportation Systems*, 2022.
- [2] Radovan Miucic. *Connected vehicles: Intelligent transportation systems*. Springer, 2018.
- [3] Keyvan Golestan, Ridha Soua, Fakhri Karray, and Mohamed S Kamel. Situation awareness within the context of connected cars: A comprehensive review and recent trends. *Information Fusion*, 29:68–83, 2016.
- [4] Shahram Rezaei, Raja Sengupta, H. Krishnan Hariharan, Xu Guan, and Raman Bhatia. Tracking the position of neighboring vehicles using wireless communications. *Transportation Research Part C: Emerging Technologies*, 2010.
- [5] Ruifeng Zhang, Libo Cao, Shan Bao, and Jianjie Tan. A method for connected vehicle trajectory prediction and collision warning algorithm based on V2V communication. *International Journal of Crashworthiness*, 2017.
- [6] Rodolfo Valiente, Mahdi Zaman, Sedat Ozer, and Yaser P Fallah. Controlling steering angle for cooperative self-driving vehicles utilizing cnn and lstm-based deep networks. In *2019 IEEE intelligent vehicles symposium (IV)*, pages 2423–2428. IEEE, 2019.
- [7] Mahdi Razzaghpour, Shahriar Shahram, Rodolfo Valiente, and Yaser P Fallah. Impact of communication loss on mpc based cooperative adaptive cruise control and platooning. *arXiv preprint arXiv:2106.09094*, 2021.
- [8] Rodolfo Valiente, Arash Raftari, Mahdi Zaman, Yaser Pourmohammadi Fallah, and Syed Mahmud. Dynamic object map based architecture for robust cvs systems. Technical report, SAE Technical Paper, 2020.
- [9] Ghayoor Shah, Rodolfo Valiente, Nitish Gupta, S M Gani, Behrad Toghi, Yaser P Fallah, and Somak Datta Gupta. Real-Time Hardware-In-the-Loop Emulation Framework for DSRC-based Connected Vehicle Applications. *arXiv preprint arXiv:1905.09267*, 2019.
- [10] Behrad Toghi, Md Saifuddin, Hossein Nourkhiz Mahjoub, MO Mughal, Yaser P Fallah, Jayanthi Rao, and Sushanta Das. Multiple access in cellular v2x: Performance analysis in highly congested vehicular networks. In *2018 IEEE Vehicular Networking Conference (VNC)*, pages 1–8. IEEE, 2018.

- [11] Yaser P. Fallah and Masoumeh K. Khandani. Analysis of the coupling of communication network and safety application in cooperative collision warning systems. 2015.
- [12] Yaser P. Fallah and Masoumeh K. Khandani. Context and Network Aware Communication Strategies for Connected Vehicle Safety Applications. *IEEE Intelligent Transportation Systems Magazine*, 2016.
- [13] F Ahmed-Zaid, F Bai, S Bai, C Basnayake, B Bellur, S Brovold, G Brown, L Caminiti, D Cunningham, H Elzein, et al. Vehicle safety communications—applications (vsc-a) final report. Technical report, 2011.
- [14] Eric Thorn, Shawn C Kimmel, Michelle Chaka, Booz Allen Hamilton, et al. A framework for automated driving system testable cases and scenarios. Technical report, United States. Department of Transportation. National Highway Traffic Safety . . . , 2018.
- [15] James A Misener, Raja Sengupta, and Hariharan Krishnan. Cooperative collision warning: Enabling crash avoidance with wireless technology. In *12th World Congress on ITS*, volume 3. Citeseer, 2005.
- [16] Feng Lyu, Hongzi Zhu, Nan Cheng, Haibo Zhou, Wenchao Xu, Minglu Li, and Xuemin Shen. Characterizing urban vehicle-to-vehicle communications for reliable safety applications. *IEEE Transactions on Intelligent Transportation Systems*, 21(6):2586–2602, 2019.
- [17] K. Lee and H. Peng. Evaluation of automotive forward collision warning and collision avoidance algorithms. *Vehicle System Dynamics*, 2005.
- [18] Changseob Kim, Jongwon Park, and Kunsoo Huh. Target classification layer design via vehicle-to-vehicle communication. *Proceedings of the Institution of Mechanical Engineers, Part D: Journal of Automobile Engineering*, 2016.
- [19] Raja Sengupta, Shahram Rezaei, Steven E. Shladover, Delphine Cody, Susan Dickey, and Hariharan Krishnan. Cooperative collision warning systems: Concept definition and experimental implementation. *Journal of Intelligent Transportation Systems: Technology, Planning, and Operations*, 2007.
- [20] Ahura Jami, Mahdi Razzaghpour, Hussein M. Alnuweiri, and Yaser P. Fallah. Augmented driver behavior models for high-fidelity simulation study of crash detection algorithms. 2022.
- [21] Lanhang Ye and Toshiyuki Yamamoto. Evaluating the impact of connected and autonomous vehicles on traffic safety. *Physica A: Statistical Mechanics and its Applications*, 526:121009, 2019.
- [22] G.J. Forkenbrock and B.C. O’Hara. A Forward Collision Warning (FCW) Performance Evaluation. *Enhanced Safety of Vehicles*, 2009.
- [23] A. Hamish Jamson, Frank C.H. Lai, and Oliver M.J. Carsten. Potential benefits of an adaptive forward collision warning system. *Transportation Research Part C: Emerging Technologies*, 2008.
- [24] R.J. Kiefer, M.T. Cassar, C.A. Flannagan, D.J. LeBlanc, M.D. Palmer, R.K. Deering, and M.A. Shulman. Forward Collision Warning Requirements Project: Refining the CAMP Crash Alert Timing Approach by Examining “Last-Second” Braking and Lane Change Maneuvers Under Various Kinematic Conditions. Technical report, 2003.
- [25] Derek Caveney. Cooperative vehicular safety applications. *IEEE Control Systems Magazine*, 30(4):38–53, 2010.
- [26] Amin Tahmasbi-Sarvestani, Hossein Nourkhiz Mahjoub, Yaser P Fallah, Ehsan Moradi-Pari, and Oubada Abuhaar. Implementation and evaluation of a cooperative vehicle-to-pedestrian safety application. *IEEE Intelligent Transportation Systems Magazine*, 9(4):62–75, 2017.
- [27] M Sepulcre, J Gozalvez, and J Hernandez. Cooperative vehicle-to-vehicle active safety testing under challenging conditions. *Transportation research part C: emerging technologies*, 26:233–255, 2013.
- [28] K Lee and H Peng. Evaluation of automotive forward collision warning and collision avoidance algorithms. *Vehicle system dynamics*, 43(10):735–751, 2005.
- [29] Xiuzhang Cai, Michael Giallorenzo, and Kamal Sarabandi. Machine learning-based target classification for mmw radar in autonomous driving. *IEEE Transactions on Intelligent Vehicles*, 6(4):678–689, 2021.
- [30] Ryan Parker and Shahrokh Valaee. Cooperative vehicle position estimation. In *IEEE International Conference on Communications*, 2007.
- [31] Stanley Baek, Chang Liu, Paul Watta, and Yi Lu Murphey. Accurate vehicle position estimation using a Kalman filter and neural network-based approach. In *2017 IEEE Symposium Series on Computational Intelligence (SSCI)*, pages 1–8. IEEE, 2017.
- [32] John H Painter, David Kerstetter, and Steve Jowers. Reconciling steady-state Kalman and alpha-beta filter design. 1990.
- [33] Liang Chu, Yanru Shi, Yongsheng Zhang, Hongwei Liu, and Mingfa Xu. Vehicle lateral and longitudinal velocity estimation based on adaptive kalman filter. In *ICACTE 2010 - 2010 3rd International Conference on Advanced Computer Theory and Engineering, Proceedings*, 2010.
- [34] H. N. Mahjoub, B. Toghi, S. M. O. Gani, and Y. P. Fallah. V2X system architecture utilizing hybrid gaussian process-based model structures. In *2019 IEEE International Systems Conference (SysCon)*, pages 1–7, April 2019.
- [35] Y. P. Fallah. A model-based communication approach for distributed and connected vehicle safety systems. In *2016 Annual IEEE Systems Conference (SysCon)*, pages 1–6, April 2016.
- [36] Jeremy Morton, Tim A Wheeler, and Mykel J Kochenderfer. Analysis of recurrent neural networks for probabilistic modeling of driver behavior. *IEEE Transactions on Intelligent Transportation Systems*, 18(5):1289–1298, 2016.
- [37] Alexandre Alahi, Vignesh Ramanathan, Krathar Goel, Alexandre Bicquet, Amir A Sadeghian, Li Fei-Fei, and Silvio Savarese. Learning to predict human behavior in crowded scenes. In *Group and Crowd Behavior for Computer Vision*, pages 183–207. Elsevier, 2017.
- [38] Kamalika Das and Ashok N Srivastava. Block-gp: Scalable gaussian process regression for multimodal data. In *2010 IEEE International Conference on Data Mining*, pages 791–796. IEEE, 2010.
- [39] Jack M Wang, David J Fleet, and Aaron Hertzmann. Gaussian process dynamical models for human motion. *IEEE transactions on pattern analysis and machine intelligence*, 30(2):283–298, 2007.
- [40] Dong Guan, Hui Zhao, Long Zhao, and Kan Zheng. Intelligent prediction of mobile vehicle trajectory based on space-time information. In *2019 IEEE 89th Vehicular Technology Conference (VTC2019-Spring)*, pages 1–5. IEEE, 2019.
- [41] Florent Alché and Arnaud de La Fortelle. An lstm network for highway trajectory prediction. In *2017 IEEE 20th international conference on intelligent transportation systems (ITSC)*, pages 353–359. IEEE, 2017.
- [42] Ian Goodfellow, Jean Pouget-Abadie, Mehdi Mirza, Bing Xu, David Warde-Farley, Sherjil Ozair, Aaron Courville, and Yoshua Bengio. Generative adversarial nets. *Advances in neural information processing systems*, 27, 2014.
- [43] Kihyuk Sohn, Honglak Lee, and Xinchen Yan. Learning structured output representation using deep conditional generative models. *Advances in neural information processing systems*, 28, 2015.
- [44] Rodolfo Valiente, Mahdi Razzaghpour, Behrad Toghi, Ghayoor Shah, and Yaser P Fallah. Prediction-aware and reinforcement learning based altruistic cooperative driving. *arXiv preprint arXiv:2211.10585*, 2022.
- [45] Behrad Toghi, Rodolfo Valiente, Dorsa Sadigh, Ramtin Pedarsani, and Yaser P Fallah. Social coordination and altruism in autonomous driving. *IEEE Transactions on Intelligent Transportation Systems*, 2022.
- [46] Behrad Toghi, Rodolfo Valiente, Ramtin Pedarsani, and Yaser P Fallah. Towards learning generalizable driving policies from restricted latent representations. *arXiv preprint arXiv:2111.03688*, 2021.
- [47] Marion Neumeier, Michael Betsch, Andreas Tollkühn, and Thomas Berberich. Variational autoencoder-based vehicle trajectory prediction with an interpretable latent space. In *2021 IEEE International Intelligent Transportation Systems Conference (ITSC)*, pages 820–827. IEEE, 2021.
- [48] Carl Edward Rasmussen. Gaussian processes in machine learning. In *Summer School on Machine Learning*, pages 63–71. Springer, 2003.
- [49] Sahand Mosharafian, Mahdi Razzaghpour, Yaser P. Fallah, and Javad Mohammadpour Velni. Gaussian process based stochastic model predictive control for cooperative adaptive cruise control. In *2021 IEEE Vehicular Networking Conference (VNC) (IEEE VNC 2021)*, Ulm, Germany, November 2021.
- [50] Mahdi Razzaghpour, Sahand Mosharafian, Arash Raftari, Javad Mohammadpour Velni, and Yaser P. Fallah. Impact of information flow topology on safety of tightly-coupled connected and automated vehicle platoons utilizing stochastic control. In *(ECC 2022)*.
- [51] Hossein Nourkhiz Mahjoub, Arash Raftari, Rodolfo Valiente, Yaser P Fallah, and Syed K Mahmud. Representing Realistic Human Driver Behaviors using a Finite Size Gaussian Process Kernel Bank.
- [52] Safety pilot model deployment dataset. <https://www.its.dot.gov/factsheets/pdf/SafetyPilotModelDeployment.pdf>. Accessed: 2019-11-29.
- [53] Carl Edward Rasmussen and Christopher K. I. Williams. *Gaussian Processes for Machine Learning*. The MIT Press, 2006.
- [54] Vicki L Neale, Thomas A Dingus, Sheila G Klauer, Jeremy Sudweeks, and Michael Goodman. An overview of the 100-car naturalistic study and findings. *National Highway Traffic Safety Administration, Paper*, 5:400, 2005.
- [55] Qi Yang, Haris N. Koutsopoulos, and Moshe E. Ben-Akiva. Simulation Laboratory for Evaluating Dynamic Traffic Management Systems. *Transportation Research Record: Journal of the Transportation Research Board*, 2007.